Contribution from the Centro di Studio per la Sintesi e la Struttura dei Composti dei Metalli di Transizione nei Bassi Stati di Ossidazione, CNR, and the Dipartimento di Chimica Inorganica e Metallorganica and Istituto di Chimica Strutturistica Inorganica, Università di Milano, Via G. Venezian 21, 20133 Milano, Italy

Reactivity of $Rh_4(CO)_{12}$ with Halides or Pseudohalides: Synthesis of the Pentanuclear Carbonyl Clusters $[Rh_5(CO)_{14}X]^{n-}$ (X = Cl, Br, I, SCN, n = 2; X = PPh_3, n = 1). Crystal Structures of $[N(PPh_3)_2][Rh_5(\mu\text{-}CO)_6(CO)_8(PPh_3)]$ and $[N(PPh_3)_2]_2[Rh_5(\mu\text{-}CO)_6(CO)_8(SCN)]$

Alessandro Fumagalli,*[1a] Secondo Martinengo,[1b] Daniele Galli,[1b] Claudio Allevi,[1b] Gianfranco Ciani,[1c] and Angelo Sironi*[1c]

Received April 20, 1989

The reaction of $Rh_4(CO)_{12}$ with salts of $[X]^-$ (X = Cl, Br, I, SCN) under CO yields salts of the dianionic species $[Rh_5(CO)_{14}X]^{2-}$. These can also be produced, together with salts of $[Rh_5(CO)_{14}(PPh_3)]^-$, by nucleophilic substitution on salts of the anionic substrate $[Rh_5(CO)_{15}]^-$. All of these 76 cluster valence electron derivatives are stable under 1 atm of CO but decompose under nitrogen or in a vacuum. the X-ray structural analysis of the $[PPN]^+$, (μ-nitrido)bis(triphenylphosphorus)(1+), salts of $[Rh_5(CO)_{14}(PPh_3)]^-$ (I) and $[Rh_5(CO)_{14}(SCN)]^{2-}$ (II), revealed in both anions an elongated trigonal-bipyramidal metallic frame, with eight terminal and six edge-bridging carbonyls; the entering group is bond to an apical rhodium. Crystal data for I: $C_{68}H_{45}NO_{14}P_3Rh_5$, fw = 1707.6, monoclinic, $P2_1/c$ (No. 14), a = 21.707 (4) Å, b = 17.054 (2) Å, c = 19.815 (4) Å, β = 114.67 (2)°, Z = 4, final R = 0.041, R_w = 0.050. Crystal data for II: $C_{87}H_{60}N_3O_{14}P_4Rh_5S$, fw = 2041.9, monoclinic, $P2_1/c$ (No. 14), a = 25.877 (6) Å, b = 15.115 (3) Å, c = 22.776 (6) Å, β = 93.95 (2)°, Z = 4, final R = 0.069, R_w = 0.092.

Introduction

Some years ago, we reported the preliminary results on the synthesis of salts of the $[Rh_5(CO)_{14}I]^{2-}$ dianion by reaction of $Rh_4(CO)_{12}$ with salts of the iodide anion.[2] Later on, the $[PPN]^+$, (μ-nitrido)bis(triphenylphosphorus)(1+), salt of a species, whose nature had remained for a long time puzzling, was isolated and characterized as $[PPN][Rh_5(CO)_{15}]$.[3] Both anions have a trigonal-bipyramidal framework and, as most of these species with 76 CVEs (cluster valence electron), are stable only under a CO atmosphere. We can now report that the reaction under CO of $Rh_4(CO)_{12}$ with various salts of a generic $[X]^-$ halide or pseudohalide yields the corresponding salt of $[Rh_5(CO)_{14}X]^{2-}$ (X = Cl, Br, I, SCN); all these products can also be obtained by nucleophilic substitution on $[Rh_5(CO)_{15}]^-$ with the proper $[X]^-$ anion. $[Rh_5(CO)_{15}]^-$ undergoes substitution also by a neutral ligand, as in the case of PPh_3, yielding $[Rh_5(CO)_{14}(PPh_3)]^-$. This new family joins the well-known series $[Rh_6(CO)_{15}X]^-$ (X = Cl, Br, I, CN, SCN, COOR, CONHR,[4] COR,[5] H[6]) and $[Rh_7(CO)_{16}X]^{2-}$ (X = Cl, Br, I),[7] which are based on octahedral and capped-octahedral metal frames, respectively.

It is also worth mentioning that $[Rh_5(CO)_{15}]^-$ has been identified in systems that catalyze the synthesis of ethylene glycol from CO/H_2,[8] and more recently some of these substituted species have been reported to be involved in the hydroformylation of formaldehyde to give glycolaldehyde.[9]

Results

1. Synthesis of $[Rh_5(CO)_{14}X]^{n-}$ (X = Cl, Br, I, SCN, n = 2; X = PPh_3, n = 1). $[Rh_5(CO)_{14}I]^{2-}$[2] was originally obtained from $Rh_4(CO)_{12}$ and $[N\text{-}n\text{-}Bu_4]I$, which were reacted under CO in 2-propanol according to the stoichiometry in (1). The product

$$3Rh_4(CO)_{12} + 6[N\text{-}n\text{-}Bu_4]I \rightarrow 2[N\text{-}n\text{-}Bu_4]_2[Rh_5(CO)_{14}I] + 2[N\text{-}n\text{-}Bu_4][Rh(CO)_2I_2] + 4CO \quad (1)$$

separates as a precipitate from the reaction mixture. Reaction 1 works similarly also in THF solution with a generic $[X]^-$ halide or pseudohalide, yielding, within minutes at room temperature, the corresponding $[Rh_5(CO)_{14}X]^{2-}$ and $[Rh(CO)_2X_2]^-$ species. A close study of the reaction course, performed by stepwise addition of the halide ions, indicated that it consists of two distinct stages. The first step is a disproportionation according to the stoichiometry

$$3Rh_4(CO)_{12} + 4[X]^- \rightarrow 2[Rh_5(CO)_{15}]^- + 2[Rh(CO)_2X_2]^- + 2CO \quad (2)$$

and the second one is a nucleophilic substitution that is best formulated as an equilibrium:

$$[Rh_5(CO)_{15}]^- + [X]^- \rightleftharpoons [Rh_5(CO)_{14}X]^{2-} + CO \quad (3)$$

Both reactions can be independently verified by setting up the proper stoichiometries.

It is worth noting, with reference to eq 2, that with a deficiency of $[X]^-$, for instance with the two reagents in a 1:1 molar ratio, the same products are obtained, with some $Rh_4(CO)_{12}$ left unreacted. Very likely, the driving forces of this reaction are both the formation of the stable $[Rh(CO)_2X_2]^-$ complex and the stabilization under CO of $[Rh_5(CO)_{15}]^-$.[3] With reference to this latter argument, it must be noted that these same reactions performed under nitrogen atmosphere yield $[Rh_6(CO)_{15}X]^-$[4] and, in the case of $[SCN]^-$, eventually $[Rh_{10}S(CO)_{22}]^{2-}$[10] and $[Rh_3S_2(CO)_6]^-$.[11]

Concerning reaction 3, stepwise addition of [PPN]X or $[NR_4]X$ to a THF solution of $[Rh_5(CO)_{15}]^-$ gives immediately the substituted dianion without evidence of other products. The completeness of this reaction is however dependent on the solvent and/or the cation.[12] There is in fact IR evidence that the reaction, shifted toward the right side in THF, upon addition of hydroxilic solvents (H_2O, CH_3OH, 2-propanol), sometimes even in a trace amount, can reverse back to the left side. This effect, which is relevant in the case of the chloride and bromide ligands, is less evident or absent in the case of iodide and thiocyanate. The relative stability of the substituted dianions in THF–hydroxilic solvent mixtures can be scaled as follows: SCN ≃ I > Br > Cl.

(1) (a) CNR. (b) Dipartimento di Chimica Inorganica e Metallorganica, Università di Milano. (c) Istituto di Chimica Strutturistica Inorganica, Università di Milano.
(2) Martinengo, S.; Ciani, G.; Sironi, A. *J. Chem. Soc., Chem. Commun.* **1979**, 1059.
(3) Fumagalli, A.; Koetzle, T. F.; Takusagawa, F.; Chini, P.; Martinengo, S.; Heaton, B. T. *J. Am. Chem. Soc.* **1980**, *102*, 1740.
(4) Chini, P.; Martinengo, S.; Giordano, G. *Gazz. Chim. Ital.* **1972**, *102*, 330.
(5) Ciani, G.; Sironi, A.; Chini, P.; Martinengo, S. *J. Organomet. Chem.* **1981**, *213*, C37.
(6) Heaton, B. T.; Strona, L.; Martinengo, S.; Strumolo, D.; Goodfellow, R. J.; Sadler, I. H. *J. Chem. Soc., Dalton Trans.* **1982**, 1499.
(7) Martinengo, S.; Chini, P.; Giordano, G.; Ceriotti, A.; Albano, V. G.; Ciani, G. *J. Organomet. Chem.* **1975**, *88*, 375.
(8) Vidal, J. L.; Walker, W. E. *Inorg. Chem.* **1980**, *19*, 896.
(9) Marchionna, M.; Longoni, G. *J. Chem. Soc., Chem. Commun.* **1987**, 1097 and references therein.
(10) Garlaschelli, L.; Fumagalli, A.; Martinengo, S.; Heaton, B. T.; Smith, D. O.; Strona, L. *J. Chem. Soc., Dalton Trans.* **1982**, 2265.
(11) Galli, D.; Garlaschelli, L.; Ciani, G.; Fumagalli, A.; Martinengo, S.; Sironi, A. *J. Chem. Soc., Dalton Trans.* **1984**, 55.
(12) Lavigne, G.; Kaesz, H. D. *J. Am. Chem. Soc.* **1984**, *106*, 4647.

0020-1669/90/1329-1408$02.50/0

Table I. IR Data in THF Solution[a]

compd	cation	CO stretchings						
$[Rh_5(CO)_{15}]^-$	PPN^+	2043 s	2010 vs	1871 mw	1842 ms	1787 m		
$[Rh_5(CO)_{14}(PPh_3)]^-$	PPN^+	2061 w	2036 s	1994 vs	1832 ms	1775 m		
$[Rh_5(CO)_{14}Cl]^{2-}$	PPN^+	2059 w	2022 s	1979 vs	1828 ms	1822 sh	1767 m	1753 mw
$[Rh_5(CO)_{14}Br]^{2-}$	PPN^+	2053 w	2022 s	1977 vs	1827 ms	1768 m	1756 mw	
	$N\text{-}n\text{-}Bu_4^+$	2057 w	2025 s	1983 vs	1828 ms	1765 m		
$[Rh_5(CO)_{14}I]^{2-}$	PPN^+	2053 w	2022 s	1977 vs	1825 ms	1766 m		
	$N\text{-}n\text{-}Bu_4^+$	2052 w	2025 s	1981 vs	1828 ms	1767 m		
$[Rh_5(CO)_{14}(SCN)]^{2-}$	PPN^+	2094 w	2058 w	2018 s	1979 vs	1828 ms	1768 m	

[a] Wavenumbers are in cm^{-1} (± 3 cm^{-1}); vs = very strong, s = strong, m = medium, w = weak, and sh = shoulder.

However, when one goes from THF–alcohol mixtures to the neat alcoholic solvent, the SCN and I derivatives are also affected. We could in fact observe that setting up a stoichiometry like (1) with NaI or $[NMe_4]I$ in methanol, as well as with KSCN in 2-propanol, results in the simple disproportionation process in (2) with little or no evidence of the subsequent substitution step, which is immediate and almost quantitative in THF. These alcoholic solution systems eventually evolve as in the above-mentioned reactions performed under a nitrogen atmosphere. In these cases the determinant is the lack of precipitation of the substituted dianion; in fact, the use of salts of bulky cations such as $[N\text{-}n\text{-}Bu_4]^+$ and $[PPN]^+$ with the same $[X]^-$, as was the case in reaction 1, yields products insoluble in the reaction medium and shifts equilibrium 3 to the right. A moderate excess of $[X]^-$ also helps in shifting this same equilibrium, with no evidence in any case of further reaction.

Because of these equilibria, the SCN and I derivatives with bulky countercations can be recovered by precipitation with 2-propanol and even recrystallized by the slow diffusion of this solvent into THF solutions, while the products of substitution with Br and Cl must be precipitated with inert solvents, such as *n*-hexane or *n*-heptane in anhydrous conditions. The pure isolated dianions, however, when dissolved in THF always give some dissociation to $[Rh_5(CO)_{15}]^-$ and $[X]^-$, as evidenced by subtractive IR techniques.

The reaction of $[Rh_5(CO)_{15}]^-$ in THF with a neutral ligand, such as triphenylphosphine, is also immediate, with remarkable CO evolution and change of the color from red to yellow-orange. At the 1:1 molar ratio there is a clean monosubstitution:

$$[Rh_5(CO)_{15}]^- + PPh_3 \rightarrow [Rh_5(CO)_{14}(PPh_3)]^- + CO \quad (4)$$

The substitution of one CO ligand gives a shift to lower wavenumbers of the CO stretching bands in the IR spectrum, according to the stronger basicity and lower π-acceptor ability of PPh_3 with respect to CO. Addition of excess phosphine causes further substitution, to give green or brown solutions from which unfortunately no crystalline product was obtained.

The phosphine can also displace the $[X]^-$ ligand (X = I, Br), according to reaction 5. A similar behavior has been already

$$[Rh_5(CO)_{14}X]^{2-} + PPh_3 \rightarrow [Rh_5(CO)_{14}(PPh_3)]^- + [X]^- \quad (5)$$

observed in the case of the $[Ir_4(CO)_{11}X]^-$ anions, and used for the synthesis of the neutral $[Ir_4(CO)_{11}L]$ (L = substituted phosphine) derivatives.[13]

All of the described compounds are air-sensitive and must be handled and stored under CO atmosphere; vacuum drying should be as short as possible. In fact, they decompose even in nitrogen or vacuum, both in solution and as finely powdered solids, generally yielding $[Rh_6(CO)_{15}X]^-$[4] in mixture with other unidentified products. The requirement of a CO atmosphere is a peculiarity of these 76 CVEs pentanuclear species.[2,3,14-18]

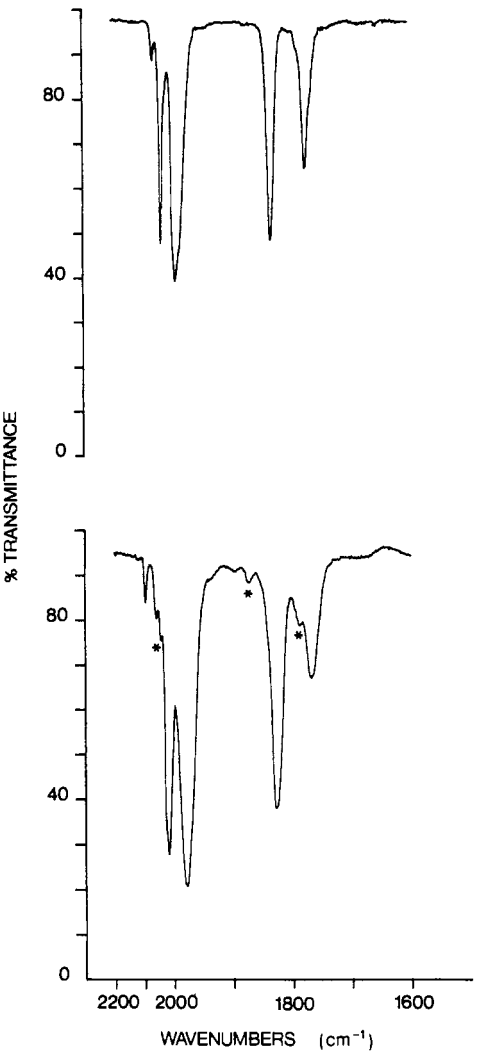

Figure 1. IR spectra in THF of $[PPN][Rh_5(CO)_{14}(PPh_3)]$ (top) and $[PPN]_2[Rh_5(CO)_{14}(SCN)]$ (bottom). The absorptions marked with an asterisk indicate an impurity of $[PPN][Rh_5(CO)_{15}]$.

The IR spectral frequencies in the CO stretching region of all the derivatives are reported in Table I, while reference spectra of $[PPN][Rh_5(CO)_{14}(PPh_3)]$ and $[PPN]_2[Rh_5(CO)_{14}(SCN)]$ in THF are reported in Figure 1. All the spectra show, in the terminal CO stretching region, the pattern with two strong bands that is characteristic of all these trigonal-bipyramidal pentanuclear clusters. It has also to be remarked that a few weak bands, as those indicated in Figure 1 (bottom), can be assigned by subtractive IR techniques to some $[Rh_5(CO)_{15}]^-$ derived from partial dissociation, which occurs according to eq 3.

2. Structures of $[PPN][Rh_5(CO)_{14}(PPh_3)]$ and $[PPN]_2[Rh_5(CO)_{14}(SCN)]$. The structures of the anions are reported in Figures 2 and 3; selected bonding parameters are given in Table II.

(13) Ros, R.; Scrivanti, A.; Albano, V. G.; Braga, D.; Garlaschelli, L. *J. Chem. Soc., Dalton Trans.* **1986**, 2411.
(14) Ceriotti, A.; Longoni, G.; Della Pergola, R.; Heaton, B. T.; Smith, D. O. *J. Chem. Soc., Dalton Trans.* **1983**, 1433.
(15) Fumagalli, A.; Ciani, G. *J. Organomet. Chem.* **1984**, *272*, 91.
(16) Fumagalli, A.; Koetzle, T. F.; Takusagawa, F. *J. Organomet. Chem.* **1981**, *213*, 365.
(17) Fumagalli, A.; Martinengo, S.; Chini, P.; Galli, D.; Heaton, B. T.; Della Pergola, R. *Inorg. Chem.* **1984**, *23*, 2947.
(18) Fumagalli, A.; Della Pergola, R.; Bonacina, F.; Garlaschelli, G.; Moret, M.; Sironi, A. *J. Am. Chem. Soc.* **1989**, *111*, 165.

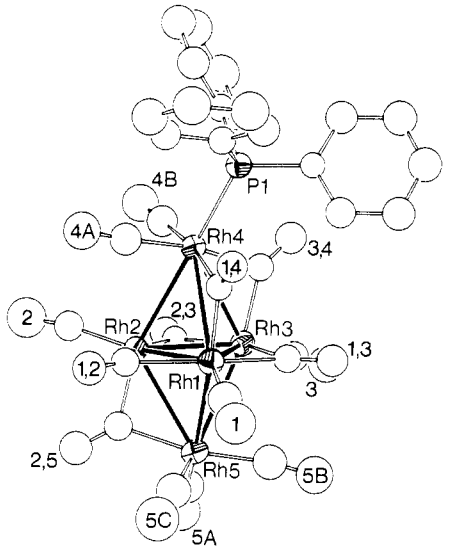

Figure 2. View of the anion $[Rh_5(\mu\text{-}CO)_6(CO)_8(PPh_3)]^-$. The carbonyl ligands are indicated by the numbers of their oxygen atoms.

Both species contain the elongated trigonal-bipyramidal metal skeleton typical of all the 76 CVE pentanuclear clusters and have a similar (*not* identical) disposition of the ligands with eight terminal and six edge-bridging CO; the substituent ligand is terminally bonded at an apical Rh atom. Three out of the six edge-bridging carbonyls, span symmetrically the edges of the equatorial metal triangle, while the other ones are positioned between the apical metals and this same triangle with the Rh_{eq}–C interactions remarkably shorter than the Rh_{ap}–C ones. The substituted Rh atom bears two such bridges. A similar $M_5(\mu\text{-}CO)_6$ moiety, with idealized C_s symmetry, has been found also in the dianions $[FeRh_4(CO)_{15}]^{2-}$,[14] $[RuRh_4(CO)_{15}]^{2-}$,[15] $[RuIr_4(CO)_{15}]^{2-}$,[16] and $[Rh_5(CO)_{14}I]^{2-}$, which has a stereochemistry similar to that of the SCN derivative. In all these species the M_{eq}–M_{eq} edge, which is unique under this ideal symmetry, is shorter than the other two. On the contrary in $[Rh_5(CO)_{15}]^-$,[3] $[PtRh_4(CO)_{14}]^{2-}$,[17] and $[PtIr_4(CO)_{14}]^{2-}$,[18] which contain a $M_5(\mu\text{-}CO)_5$ moiety with (crystallographic) C_2 symmetry, the unique edge of the equatorial triangle has been found to be longer than the two symmetry-related ones. This latter stereochemical type imposes equivalence of the two apical metal atoms, each bearing four coordinated ligands, while in the case of a disposition of the bridging carbonyl ligands according to the C_s symmetry, the two apical metals are unequivalent, bearing four and five ligands respectively. The C_s stereochemistry of both I and II can be seen as derived from that of the parent $[Rh_5(CO)_{15}]^-$ (C_2) by tilting one of the two geminal carbonyls in the equatorial triangle to bridge the substituted metal apex, which thus bears five ligands.

In the $[Rh_5(CO)_{14}(SCN)]^{2-}$ anion, the sulfur-bonded SCN moiety (S–C–N = 172 (2)°; Rh–S–C = 105.5 (8)°) is trans to a bridging carbonyl group, analogous to what was found in the iodo derivative.[2] This geometry is postulated also for the Cl- and Br-containing species on the basis of very similar IR spectra.

In the $[Rh_5(CO)_{14}(PPh_3)]^-$ anion, the PPh_3 ligand is also bound on the more crowded apical position but trans to the unbridged M_{eq}–M_{ap} bond, i.e. far away from the equatorial triangle. This specific preference within the $Rh(CO)_4L$ apical fragment must be related to the bulkiness of the PPh_3 ligand, which also causes significant lengthening of the three relative M_{eq}–M_{ap} interactions. The mean values of the M_{eq}–M_{ap} bond lengths in $[Rh_5(CO)_{14}(PPh_3)]^-$, $[Rh_5(CO)_{14}(SCN)]^{2-}$, and $[Rh_5(CO)_{14}I]^{2-}$ are, in fact, 3.011, 2.983, and 2.983 Å for the substituted Rh atom and 2.975, 2.976, and 2.974 Å for the unsubstituted one, respectively. The M_{eq}–M_{ap} average value in the parent $[Rh_5(CO)_{15}]^-$ is 2.967 Å.

Conclusions

The selectivity of the nucleophilic substitution in the apical positions of the $[Rh_5(CO)_{15}]^-$ anion can be explained, in the case of the bulky phosphine ligand, with sterical requirements that cannot be invoked for the SCN^- and I^- ligands. Therefore other factors, presumably electronic or kinetic, are driving the entering ligand at the apical site. At present we have no data to decide which effect could be predominant. In any case, without any reference to the site of the initial nucleophilic attack and the details of the mechanism, the apical position seems more suitable to bear ligands that, because of their donor–acceptor properties, transfer more charge than CO onto the metal. In fact, the net and somewhat surprising result of the substitution is an increased coordination of ligands at the metal center, from four to five. To achieve this, a carbonyl, originally terminal on an equatorial Rh of $[Rh_5(CO)_{15}]^-$, comes to bridge the substituted apical position. This increase of coordination is probably necessary to allow a better delocalization of the charge donated by the entering ligand, and very likely, such an high crowding of ligands would not be possible around an equatorial rhodium because of sterical hindrance.

Table II. Selected Bond Distances (Å) within the $[Rh_5(CO)_{14}PPh_3]^-$ and $[Rh_5(CO)_{14}SCN]^{2-}$ Anions

	$[Rh_5(CO)_{14}PPh_3]^-$	$[Rh_5(CO)_{14}SCN]^{2-}$
Rh1–Rh2	2.715 (1)	2.713 (2)
Rh1-Rh3	2.675 (1)	2.674 (2)
Rh2–Rh3	2.727 (1)	2.718 (2)
Rh1–Rh4	3.022 (1)	3.000 (1)
Rh2–Rh4	3.003 (1)	2.978 (2)
Rh3–Rh4	3.008 (1)	2.972 (2)
Rh1–Rh5	3.002 (1)	2.960 (2)
Rh2–Rh5	2.933 (1)	2.915 (2)
Rh3–Rh5	2.989 (1)	3.053 (2)
Rh4–P1	2.382 (3)	
Rh4–S		2.582 (5)
S–C		1.60 (2)
C–N		1.21 (3)
Rh1–C1	1.86 (1)	1.85 (1)
Rh2–C2	1.84 (1)	1.83 (2)
Rh3–C3	1.85 (1)	1.87 (1)
Rh4–C4A	1.91 (1)	1.95 (2)
Rh4–C4B	1.92 (1)	1.90 (2)
Rh5–C5A	1.92 (1)	1.91 (2)
Rh5–C5B	1.89 (1)	1.91 (2)
Rh5–C5C	1.88 (1)	1.78 (2)
Rh1–C1,2	2.09 (1)	2.09 (1)
Rh2–C1,2	2.05 (1)	2.06 (1)
Rh1–C1,3	2.05 (1)	2.12 (1)
Rh3–C1,3	2.09 (1)	2.05 (1)
Rh2–C2,3	2.06 (1)	2.06 (1)
Rh3–C2,3	2.11 (1)	2.07 (1)
Rh1–C1,4	1.94 (1)	1.95 (1)
Rh4–C1,4	2.13 (1)	2.09 (1)
Rh2–C2,5	1.98 (1)	1.98 (2)
Rh5–C2,5	2.02 (1)	2.05 (2)
Rh3–C3,4	1.94 (1)	1.99 (1)
Rh4–C3,4	2.16 (1)	2.08 (1)
C1–O1	1.15 (1)	1.16 (2)
C2–O2	1.18 (1)	1.19 (2)
C3–O3	1.15 (1)	1.14 (2)
C4A–O4A	1.17 (1)	1.11 (2)
C4B–O4B	1.16 (1)	1.13 (2)
C5A–O5A	1.11 (1)	1.16 (2)
C5B–O5B	1.18 (1)	1.14 (2)
C5C–O5C	1.17 (1)	1.15 (3)
C1,2–O1,2	1.19 (1)	1.17 (2)
C1,3–O1,3	1.17 (1)	1.16 (2)
C2,3–O2,3	1.17 (1)	1.20 (2)
C1,4–O1,4	1.19 (1)	1.17 (2)
C2,5–O2,5	1.22 (1)	1.23 (2)
C3,4–O3,4	1.17 (1)	1.21 (2)

Experimental Section

All the reactions and subsequent manipulations were carried out under a carbon monoxide atmosphere in carefully purified and anhydrous solvents that were stored under nitrogen. $Rh_4(CO)_{12}$[19] and [PPN]-

(19) Martinengo, S.; Giordano, G.; Chini, P. *Inorg. Synth.* **1980**, *20*, 209.

Table III. Crystallographic Data for $[(Ph_3P)_2N][Rh_5(CO)_{14}PPh_3]$ (I) and $[(Ph_3P)_2N]_2[Rh_5(CO)_{14}SCN]$ (II)

	I	II
chemical formula	$C_{68}H_{45}NO_{14}P_3Rh_5$	$C_{87}H_{60}N_3O_{14}P_4Rh_5S$
fw	1707.6	2041.9
a, Å	21.707 (4)	25.877 (6)
b, Å	17.054 (2)	15.115 (3)
c, Å	19.815 (4)	22.776 (6)
β, deg	114.67 (2)	93.95 (2)
V, Å^3	6665.8	8887.3
Z	4	4
space group	$P2_1/c$ (No. 14)	$P2_1/c$ (No. 14)
temp	room temp	room temp
λ, Å	0.71073	0.71073
ρ_{calcd}, g cm^{-3}	1.70	1.53
μ, cm^{-1}	13.26	10.47
transm coeff	1.00–0.87	
$R(F_o)$	0.041	0.069
$R_w(F_o)$	0.050	0.092

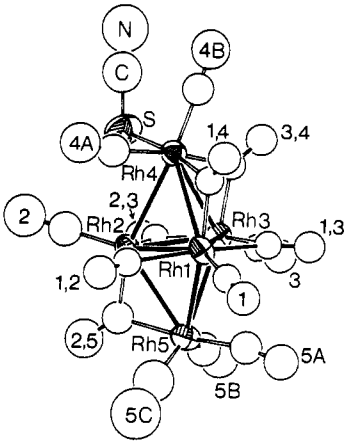

Figure 3. View of the dianion $[Rh_5(\mu\text{-}CO)_6(CO)_8(SCN)]^{2-}$. The carbonyl ligands are indicated by the numbers of their oxygen atoms.

$[Rh_5(CO)_{15}]^3$ were prepared according to the literature. Infrared spectra were recorded on a Perkin-Elmer 781 grating spectrophotometer equipped with a Data Station, using 0.1-mm calcium fluoride cells previously purged with carbon monoxide.

1. Synthesis of $[PPN]_2[Rh_5(CO)_{14}Cl]$. (a) From $Rh_4(CO)_{12}$ and [PPN]Cl. $Rh_4(CO)_{12}$ (0.460 g, 0.616 mmol) and [PPN]Cl (1.0 g, 1.74 mmol) were placed in a Schlenk tube under CO. Upon addition of THF (10 mL) and stirring, gas evolution was observed and a yellow-orange solution was obtained within minutes. The solution was filtered under CO to eliminate the excess [PPN]Cl and then carefully layered with n-heptane (20 mL). When the diffusion of the solvents was complete, the crystalline brown product was filtered under CO and washed with

Table IV. Atomic Coordinates for $[(Ph_3P)_2N][Rh_5(CO)_{14}PPh_3]$ (I)

atom	x	y	z	B,[a] Å^2	atom	x	y	z	B,[a] Å^2
Rh1	0.16804 (4)	0.03871 (5)	0.82642 (5)	3.29 (2)	C131	−0.0572 (5)	0.1803 (7)	0.6189 (6)	3.7 (3)*
Rh2	0.21225 (4)	−0.02329 (6)	0.72836 (5)	3.13 (2)	C132	−0.0866 (6)	0.1112 (7)	0.5797 (6)	4.5 (3)*
Rh3	0.25314 (4)	0.12178 (5)	0.78830 (5)	3.19 (2)	C133	−0.1505 (7)	0.0864 (8)	0.5750 (8)	6.1 (4)*
Rh4	0.11023 (4)	0.10691 (5)	0.67150 (5)	2.91 (2)	C134	−0.1832 (7)	0.1316 (9)	0.6093 (8)	6.6 (4)*
Rh5	0.31162 (5)	−0.01881 (6)	0.88382 (5)	3.82 (2)	C135	−0.1542 (7)	0.2021 (9)	0.6475 (8)	6.9 (4)*
C1	0.1424 (6)	0.0120 (8)	0.9021 (7)	5.6 (3)*	C136	−0.0890 (6)	0.2254 (8)	0.6517 (7)	5.2 (3)*
O1	0.1285 (5)	−0.0030 (6)	0.9504 (6)	8.0 (3)*	P2	0.6331 (1)	0.4712 (2)	0.1665 (2)	3.18 (7)
C2	0.1959 (6)	−0.0865 (7)	0.6472 (6)	4.6 (3)*	P3	0.5632 (1)	0.5667 (2)	0.2415 (2)	3.48 (8)
O2	0.1946 (5)	−0.1301 (6)	0.6001 (6)	8.1 (3)*	N	0.5924 (4)	0.5378 (6)	0.1849 (5)	4.3 (2)*
C3	0.3223 (6)	0.1949 (7)	0.8197 (6)	4.7 (3)*	C211	0.6646 (5)	0.5131 (6)	0.1034 (5)	3.3 (2)*
O3	0.3648 (4)	0.2410 (6)	0.8402 (5)	6.8 (2)*	C212	0.6540 (5)	0.4731 (7)	0.0368 (6)	4.0 (3)*
C4A	0.0553 (6)	0.0164 (8)	0.6316 (7)	5.0 (3)*	C213	0.6793 (6)	0.5064 (7)	−0.0119 (6)	4.6 (3)*
O4A	0.0221 (5)	−0.0372 (6)	0.6004 (5)	6.8 (2)*	C214	0.7126 (6)	0.5758 (8)	0.0066 (7)	5.4 (3)*
C4B	0.1392 (6)	0.1054 (8)	0.5924 (7)	4.9 (3)*	C215	0.7228 (6)	0.6177 (8)	0.0712 (7)	5.7 (3)*
O4B	0.1509 (5)	0.1013 (6)	0.5406 (5)	7.0 (3)*	C216	0.6974 (6)	0.5859 (7)	0.1209 (6)	4.4 (3)*
C5A	0.4024 (6)	−0.0319 (8)	0.8914 (7)	5.6 (3)*	C221	0.7038 (5)	0.4343 (7)	0.2446 (6)	3.8 (3)*
O5A	0.4553 (5)	−0.0475 (6)	0.9015 (5)	7.9 (3)*	C222	0.6899 (6)	0.3888 (8)	0.2970 (7)	5.3 (3)*
C5B	0.3365 (7)	0.0684 (9)	0.9488 (7)	6.1 (3)*	C223	0.7446 (7)	0.3640 (9)	0.3624 (8)	6.6 (4)*
O5B	0.3615 (5)	0.1179 (6)	0.9932 (5)	7.1 (3)*	C224	0.8102 (7)	0.3826 (9)	0.3759 (8)	7.2 (4)*
C5C	0.2803 (7)	−0.0889 (8)	0.9357 (7)	6.0 (3)*	C225	0.8235 (8)	0.427 (1)	0.3237 (9)	8.7 (5)*
O5C	0.2659 (5)	−0.1372 (7)	0.9683 (6)	9.3 (3)*	C226	0.7694 (7)	0.4532 (8)	0.2562 (7)	6.0 (3)*
C1,2	0.1468 (6)	−0.0679 (7)	0.7689 (6)	4.0 (3)*	C231	0.5792 (5)	0.3894 (6)	0.1206 (6)	3.3 (2)*
O1,2	0.1141 (4)	−0.1252 (5)	0.7642 (4)	5.5 (2)*	C232	0.6074 (6)	0.3134 (7)	0.1314 (6)	4.7 (3)*
C1,3	0.2120 (6)	0.1458 (7)	0.8644 (6)	3.9 (3)*	C233	0.5622 (7)	0.2488 (9)	0.0934 (7)	6.1 (4)*
O1,3	0.2102 (4)	0.1958 (5)	0.9040 (4)	4.9 (2)*	C234	0.4954 (7)	0.2642 (8)	0.0487 (7)	5.9 (3)*
C1,4	0.0841 (5)	0.0897 (7)	0.7628 (6)	3.5 (2)*	C235	0.4676 (7)	0.3416 (9)	0.0374 (7)	5.8 (3)*
O1,4	0.0327 (4)	0.1058 (5)	0.7678 (4)	4.7 (2)*	C236	0.5115 (6)	0.4055 (7)	0.0745 (6)	4.5 (3)*
C2,3	0.2793 (5)	0.0540 (7)	0.7149 (6)	3.4 (2)*	C311	0.4866 (5)	0.6202 (6)	0.1899 (5)	3.2 (2)*
O2,3	0.3131 (4)	0.0599 (5)	0.6822 (4)	5.0 (2)*	C312	0.4770 (5)	0.6491 (7)	0.1206 (6)	3.7 (3)*
C2,5	0.2813 (6)	−0.0948 (7)	0.7976 (6)	4.2 (3)*	C313	0.4165 (6)	0.6912 (8)	0.0783 (7)	5.2 (3)*
O2,5	0.2966 (4)	−0.1616 (5)	0.7893 (4)	5.6 (2)*	C314	0.3672 (6)	0.6990 (8)	0.1054 (7)	5.4 (3)*
C3,4	0.1887 (5)	0.1939 (7)	0.7187 (6)	3.9 (3)*	C315	0.3773 (7)	0.6728 (9)	0.1741 (8)	6.3 (4)*
O3,4	0.1885 (4)	0.2593 (5)	0.7001 (4)	5.1 (2)*	C316	0.4379 (6)	0.6305 (8)	0.2178 (7)	5.0 (3)*
P1	0.0276 (1)	0.2084 (2)	0.6264 (2)	3.09 (7)	C321	0.5411 (5)	0.4897 (6)	0.2882 (5)	3.3 (2)*
C111	0.0134 (5)	0.2385 (7)	0.5312 (6)	3.8 (3)*	C322	0.5784 (6)	0.4754 (7)	0.3634 (6)	4.2 (3)*
C112	0.0687 (6)	0.2745 (8)	0.5238 (7)	5.6 (3)*	C323	0.5598 (6)	0.4135 (8)	0.3987 (7)	5.2 (3)*
C113	0.0621 (7)	0.2938 (9)	0.4518 (8)	7.0 (4)*	C324	0.5026 (6)	0.3662 (8)	0.3559 (7)	5.4 (3)*
C114	0.0011 (8)	0.282 (1)	0.3894 (8)	7.6 (4)*	C325	0.4659 (6)	0.3797 (7)	0.2803 (6)	4.7 (3)*
C115	−0.0553 (7)	0.2485 (9)	0.3990 (7)	6.1 (4)*	C326	0.4841 (6)	0.4435 (7)	0.2474 (7)	4.6 (3)*
C116	−0.0479 (6)	0.2280 (8)	0.4722 (7)	5.2 (3)*	C331	0.6223 (6)	0.6301 (7)	0.3099 (6)	4.2 (3)*
C121	0.0439 (5)	0.3001 (6)	0.6781 (5)	3.2 (2)*	C332	0.6904 (6)	0.6075 (8)	0.3423 (7)	5.6 (3)*
C122	0.0754 (6)	0.2977 (7)	0.7555 (6)	4.6 (3)*	C333	0.7389 (7)	0.6557 (9)	0.3977 (7)	6.2 (4)*
C123	0.0861 (6)	0.3678 (8)	0.7985 (7)	5.3 (3)*	C334	0.7170 (6)	0.7265 (8)	0.4147 (7)	5.1 (3)*
C124	0.0632 (7)	0.4379 (8)	0.7583 (7)	5.7 (3)*	C335	0.6511 (7)	0.7487 (9)	0.3825 (7)	6.2 (4)*
C125	0.0322 (7)	0.4434 (8)	0.6837 (7)	5.8 (3)*	C336	0.6006 (6)	0.6996 (8)	0.3301 (7)	5.0 (3)*
C126	0.0219 (6)	0.3725 (8)	0.6405 (7)	5.1 (3)*					

[a] Atoms with values marked with an asterisk were refined isotropically. Values for anisotropically refined atoms are given in the form of the isotropic equivalent thermal parameter defined as $(4/3)[a^2B(1,1) + b^2B(2,2) + c^2B(3,3) + ab(\cos\gamma)B(1,2) + ac(\cos\beta)B(1,3) + bc(\cos\alpha)B(2,3)]$.

Table V. Atomic Coordinates ($\times 10^4$) for $[(Ph_3P)_2N]_2[Rh_5(CO)_{14}SCN]$ (II)

atom	x/a	y/b	z/c	B, Å²	atom	x/a	y/b	z/c	B, Å²
Rh1	1698 (1)	1735 (1)	−283 (1)		C134	−1173 (5)	5360 (5)	2478 (4)	8.2 (4)
Rh2	2749 (1)	1669 (1)	−204 (1)		C135	−962 (4)	5153 (6)	3040 (4)	8.4 (4)
Rh3	2218 (1)	2102 (1)	743 (1)		C136	−755 (3)	4316 (7)	3156 (3)	6.1 (3)
Rh4	2271 (1)	3461 (1)	−193 (1)		C211	−494 (3)	817 (4)	4133 (3)	3.5 (2)
Rh5	2211 (1)	192 (1)	306 (1)		C212	−764 (2)	219 (6)	4461 (4)	5.3 (3)
S	3218 (1)	3868 (3)	127 (2)		C213	−563 (3)	−622 (5)	4576 (3)	5.8 (3)
P1	−437 (1)	2646 (2)	2883 (1)		C214	−93 (3)	−865 (4)	4363 (3)	5.6 (3)
P2	−743 (1)	1916 (2)	3999 (1)		C215	177 (2)	−267 (6)	4035 (4)	6.2 (3)
P3	−4977 (1)	1451 (2)	1648 (1)		C216	−23 (3)	574 (5)	3920 (3)	4.8 (3)
P4	−4303 (1)	1139 (2)	2733 (1)		C221	−692 (4)	2462 (6)	4694 (3)	3.8 (2)
C	3255 (8)	4919 (14)	46 (9)	10.0 (5)	C222	−1059 (3)	2322 (6)	5104 (4)	5.0 (3)
N	3280 (8)	5717 (14)	57 (9)	13.9 (6)	C223	−1010 (3)	2752 (6)	5646 (3)	7.0 (4)
C1	1096 (5)	1248 (9)	−630 (5)	4.7 (3)	C224	−596 (4)	3322 (6)	5777 (3)	6.8 (4)
O1	722 (4)	908 (7)	−823 (4)	6.5 (2)	C225	−230 (3)	3461 (6)	5367 (4)	6.2 (3)
C2	3329 (6)	1911 (11)	−588 (7)	7.3 (4)	C226	−278 (3)	3031 (6)	4825 (3)	4.8 (3)
O2	3697 (5)	2077 (10)	−857 (6)	11.2 (4)	C231	−1422 (2)	1844 (7)	3758 (4)	4.0 (2)
C3	2263 (5)	2010 (9)	1566 (6)	4.8 (3)	C232	−1715 (4)	2615 (5)	3769 (4)	5.8 (3)
O3	2292 (4)	1926 (7)	2063 (4)	7.1 (2)	C233	−2238 (4)	2599 (5)	3582 (4)	8.0 (4)
C4A	2505 (6)	3347 (11)	−984 (7)	6.6 (4)	C234	−2469 (2)	1812 (7)	3384 (4)	8.4 (4)
O4A	2606 (5)	3400 (9)	−1451 (6)	10.0 (3)	C235	−2175 (4)	1041 (5)	3372 (4)	6.9 (4)
C4B	2022 (6)	4640 (10)	−215 (6)	6.2 (3)	C236	−1652 (4)	1057 (5)	3560 (4)	6.2 (3)
O4B	1882 (5)	5350 (8)	−253 (5)	9.2 (3)	C311	−4898 (3)	2303 (5)	1104 (3)	4.3 (2)
C5A	1491 (6)	108 (11)	429 (7)	6.5 (3)	C312	−5324 (2)	2765 (6)	854 (4)	5.4 (3)
O5A	1067 (4)	−83 (7)	505 (4)	7.5 (2)	C313	−5258 (3)	3384 (5)	413 (4)	5.8 (3)
C5B	2510 (6)	38 (11)	1092 (7)	7.2 (4)	C314	−4767 (3)	3541 (5)	222 (3)	6.0 (3)
O5B	2631 (5)	−85 (8)	1577 (5)	9.3 (3)	C315	−4341 (2)	3079 (6)	472 (4)	5.7 (3)
C5C	2191 (8)	−663 (15)	−232 (9)	10.5 (6)	C316	−4407 (3)	2460 (5)	913 (4)	5.0 (3)
O5C	2168 (7)	−1280 (13)	−526 (8)	15.7 (6)	C321	−5080 (4)	433 (4)	1249 (3)	3.9 (2)
C1,2	2223 (5)	1370 (9)	−896 (6)	5.0 (3)	C322	−5443 (3)	397 (5)	769 (4)	5.0 (3)
O1,2	2209 (4)	1119 (7)	−1382 (4)	6.6 (2)	C323	−5498 (3)	−372 (5)	435 (3)	5.8 (3)
C1,3	1434 (5)	1988 (9)	561 (5)	4.7 (3)	C324	−5190 (4)	−1106 (4)	581 (3)	5.8 (3)
O1,3	1044 (3)	2027 (6)	785 (4)	5.9 (2)	C325	−4827 (3)	−1069 (5)	1061 (4)	6.3 (3)
C1,4	1549 (5)	2965 (9)	−494 (6)	4.9 (3)	C326	−4772 (3)	−300 (5)	1395 (3)	4.9 (3)
C1,4	1211 (4)	3359 (7)	−743 (4)	6.3 (2)	C331	−5552 (2)	1700 (6)	2019 (3)	3.8 (2)
C2,3	3002 (5)	1968 (9)	648 (6)	5.1 (3)	C332	−5564 (3)	2510 (5)	2308 (4)	4.7 (3)
O2,3	3407 (4)	2002 (7)	939 (4)	6.8 (2)	C333	−5986 (3)	2728 (4)	2627 (3)	5.5 (3)
C2,5	2924 (6)	423 (11)	0 (7)	6.5 (4)	C334	−6396 (2)	2136 (6)	2657 (3)	5.4 (3)
O2,5	3325 (5)	−10 (9)	−37 (5)	9.5 (3)	C335	−6383 (3)	1326 (5)	2367 (4)	5.3 (3)
C3,4	2120 (5)	3404 (9)	690 (6)	5.3 (3)	C336	−5961 (3)	1108 (4)	2048 (3)	4.3 (2)
O3,4	2002 (4)	3953 (7)	1043 (4)	6.4 (2)	C411	−4820 (3)	724 (6)	3140 (3)	4.1 (2)
N1	−402 (3)	2444 (6)	3565 (4)	4.0 (2)	C412	−5078 (3)	1294 (4)	3500 (4)	4.8 (3)
N2	−4463 (4)	1427 (7)	2070 (4)	4.5 (2)	C413	−5512 (3)	1001 (5)	3773 (3)	5.5 (3)
C111	209 (2)	2766 (7)	2666 (3)	3.3 (2)	C414	−5687 (3)	137 (6)	3685 (3)	6.1 (3)
C112	631 (3)	2654 (5)	3073 (2)	4.0 (2)	C415	−5429 (3)	−432 (4)	3325 (4)	5.8 (3)
C113	1131 (2)	2804 (6)	2906 (3)	5.0 (3)	C416	−4995 (3)	−139 (5)	3052 (3)	5.1 (3)
C114	1210 (2)	3067 (7)	2334 (3)	5.9 (3)	C421	−4026 (4)	2057 (6)	3145 (4)	4.3 (2)
C115	788 (3)	3178 (5)	1927 (2)	5.9 (3)	C422	−3842 (4)	1934 (5)	3728 (4)	5.5 (3)
C116	288 (2)	3028 (6)	2093 (3)	5.2 (3)	C423	−3615 (2)	2636 (7)	4046 (3)	7.2 (4)
C121	−752 (3)	1775 (5)	2452 (4)	3.6 (2)	C424	−3572 (4)	3460 (6)	3782 (4)	8.2 (4)
C122	−466 (2)	1015 (6)	2358 (4)	4.8 (3)	C425	−3755 (4)	3583 (5)	3199 (4)	7.9 (4)
C123	−708 (3)	275 (5)	2099 (4)	6.4 (3)	C426	−3982 (2)	2881 (7)	2880 (3)	6.4 (3)
C124	−1236 (3)	296 (5)	1935 (4)	6.2 (3)	C431	−3786 (3)	332 (6)	2726 (3)	4.1 (2)
C125	−1522 (2)	1056 (6)	2030 (4)	6.0 (3)	C432	−3506 (3)	293 (5)	2227 (3)	5.3 (3)
C126	−1281 (3)	1796 (5)	2288 (4)	5.0 (3)	C433	−3089 (3)	−285 (6)	2209 (3)	5.7 (3)
C131	−760 (5)	3685 (5)	2710 (4)	4.3 (2)	C434	−2953 (3)	−825 (6)	2690 (3)	6.1 (3)
C132	−972 (4)	3892 (6)	2148 (4)	6.2 (3)	C435	−3233 (3)	−786 (5)	3189 (3)	5.6 (3)
C133	−1178 (3)	4729 (7)	2032 (3)	7.9 (4)	C436	−3650 (3)	−207 (6)	3207 (3)	5.6 (3)

n-hexane and after a brief vacuum drying was stored under CO. The product contains small amounts of yellow crystalline $[PPN][Rh(CO)_2Cl_2]$.

(b) From $[PPN][Rh_5(CO)_{15}]$ and [PPN]Cl. $[PPN][Rh_5(CO)_{15}]$ (0.233 g, 0.175 mmol) was dissolved under CO in THF (10 mL). Upon addition of [PPN]Cl (0.103 g, 0.175 mmol), the red solution turned immediately to yellow-orange. Layering of *n*-heptane (30 mL) gave a brown crystalline product, which was recovered as in part a, with yields of about 85%.

2. Synthesis of $[N\text{-}n\text{-}Bu_4]_2[Rh_5(CO)_{14}Br]$. $Rh_4(CO)_{12}$ (0.568 g, 0.692 mmol) and $[N\text{-}n\text{-}Bu_4]Br$ (0.440 g, 1.365 mmol) were placed in a Schlenk tube under CO. THF (6 mL) was added and the mixture stirred; gas evolution was observed, while the solution turned to yellow-orange within minutes. Dropwise addition of *n*-heptane (15 mL) caused the precipitation of a reddish oily product. After decantation, the yellow mother liquor was syringed off and discarded. The residual oil was redissolved with THF (5 mL); *n*-heptane (20 mL) was carefully layered over the solution. When the diffusion of the solvents was completed, red-brown crystals of the product were recovered as in part 1.

3. Synthesis of $[N\text{-}n\text{-}Bu_4]_2[Rh_5(CO)_{14}I]$. $Rh_4(CO)_{12}$ (0.175 g, 0.234 mmol) and $[NBu_4]I$ (0.175 g, 0.474 mmol) were placed in a Schlenk tube under CO; 2-propanol (15 mL) was added and the mixture stirred for 24 h. The resulting precipitate was filtered, washed quickly with cold 2-propanol and then with *n*-hexane, and extracted from the septum with THF (5 mL). The filtered THF solution was carefully layered with a mixture of 2-propanol (30 mL) and *n*-hexane (10 mL) previously saturated with CO. When the diffusion of the solvents was completed, the crystalline product was filtered, washed twice with cold 2-propanol (5 mL) and then with *n*-hexane, and dried briefly under vacuum. The yield was about 70%.

Anal. Found (calcd) for $C_{46}H_{72}IN_2O_{14}Rh_5$: C, 35.87 (36.39); H, 4.89 (4.78); N, 1.77 (1.85).

The $[PPN]^+$ and $[PPh_4]^+$ salts were prepared in a similar manner; the yields were slightly higher, due to the lower solubility of these salts, which diminishes losses in the mother liquor and washings.

4. Synthesis of $[PPN]_2[Rh_5(CO)_{14}(SCN)]$. $[PPN][Rh_5(CO)_{15}]$ (0.312 g, 0.212 mmol) and [PPN](SCN) (0.140 g, 0.235 mmol) were placed under CO atmosphere and THF (8 mL) was added. The orange-yellow

solution obtained within a few seconds was layered with a mixture of 2-propanol and *n*-heptane (1:1 v/v, 80 mL). When the diffusion was completed, brown-red crystals of the product were recovered as in part 1, with yields of ca. 75%.

5. Synthesis of [PPN][$Rh_5(CO)_{14}(PPh_3)$]. (a) From [PPN][$Rh_5(CO)_{15}$] and PPh_3. [PPN][$Rh_5(CO)_{15}$] (0.265 g, 0.180 mmol) in THF (2.2 mL), under CO, was treated while being stirred, with PPh_3 (0.052 g, 0.198 mmol, 1.1:1). An immediate reaction was observed with CO evolution and change of the color to orange, while the IR spectrum showed quantitative formation of the $[Rh_5(CO)_{14}(PPh_3)]^-$ anion. After 1 h, the solution was cautiously layered with a mixture of 2-propanol (16 mL) and *n*-hexane (8 mL) previously saturated with CO. The product separated out initially as an oil, which eventually slowly crystallized almost completely. When the diffusion of the solvents was completed (ca. 1 week), the mother liquor was syringed off and the mixture of crystals and solidified oil was washed with 2-propanol (6 mL), then briefly vacuum-dried, and stored under CO. Both the crystals and the amorphous solid have the same IR spectrum. Though the reaction appears quantitative, some product is lost in the mother liquor, to give final yields of ca. 80-85%.

(b) By Replacement of X^- on $[PPN]_2[Rh_5(CO)_{14}X]$ (X = I, Br). A red-orange solution of $[PPN]_2[Rh_5(CO)_{14}I]$ or $[PPh_4]_2[Rh_5(CO)_{14}Br]$ (0.05 g) in THF (3 mL) under CO, was treated, while being stirred, with a slight excess of PPh_3. Immediate reaction was observed, with formation of a white precipitate and color change to orange-yellow, while the IR spectrum showed that the absorptions of the starting anions were completely replaced by those of $[Rh_5(CO)_{14}(PPh_3)]^-$. The white precipitate was recognized as [PPN]I or $[PPh_4]Br$, respectively.

6. X-ray Analysis. Crystallographic data for both compounds are reported in Table III; details of the data collection are given in the supplementary material (Table S1). Both collections were performed with crystal samples sealed under nitrogen atmosphere in a Lindemann capillary, and no decay was observed.

The structures were solved by Patterson and Fourier methods and refined by full-matrix least-squares techniques. In both cases, the metal, the phosphorus, and the sulfur atoms were refined with anisotropic thermal parameters. In the refinement of $[PPN]_2[Rh_5(CO)_{14}(SCN)]$ the phenyl rings were treated as rigid bodies of D_{6h} symmetry. The final conventional agreement factors $R = \sum(F_o - k|F_c|)/\sum F_o$ and $R_w = [\sum w(F_o - k|F_c|)^2/\sum wF_o^2]^{1/2}$ were, respectively, 0.041 and 0.050 in the PPh_3 derivative and 0.069 and 0.092 in the SCN derivative. Weights were assigned to individual observations according to the formula $w = 4F_o^2/\sigma(F_o^2)^2$, where $\sigma(F_o^2) = [\sigma(I)^2 + (pI)^2]^{1/2}/LP$ and p the "ignorance factor" is equal to 0.03. The computations were made, in the case of the PPh_3 derivative, on a PDP 11/34 computer using the Enraf-Nonius Structure Determination Package (SDP) and the physical constants therein tabulated; in the case of the SCN derivative an Univac 1100/80 computer was used with local programs.

The final positional parameters are reported in Tables IV and V.

Supplementary Material Available: Crystal data and details of the intensity measurements for both $[(Ph_3P)_2N][Rh_5(CO)_{14}PPh_3]$ (I) and $[(Ph_3P)_2N]_2[Rh_5(CO)_{14}SCN]$ (II) (Table S1) and thermal parameters for I and II (Table S2) (2 pages); two lists of computed and observed structure factor moduli (Table S3 for I and Table S4 for II) (57 pages). Ordering information is given on any current masthead page.

Contribution from the Department of Chemistry, North Carolina State University, Raleigh, North Carolina 27695-8204, and Laboratoire de Chimie des Solides, IPCM, Université de Nantes, 44072 Nantes Cedex 03, France

Structural Origin of the Electronic Instability in Titanium Bronze $Na_{0.25}TiO_2$

Michel Evain,[†] Myung-Hwan Whangbo,*[,†] Luc Brohan,[‡] and René Marchand[‡]

Received September 1, 1989

The origin of the charge density wave phenomenon in $Na_{0.25}TiO_2$ was investigated by examining the octahedral distortions in $Na_{0.25}TiO_2$ and by calculating the tight-binding band electronic structure of $Na_{0.25}TiO_2$. Despite its three-dimensional lattice, $Na_{0.25}TiO_2$ is essentially a one-dimensional metal. This finding is explained on the basis of the distortions present in the TiO_6 octahedra of the $Na_{0.25}TiO_2$ lattice.

Recently, Brohan et al have shown[1] that sodium titanium bronze $Na_{0.25}TiO_2$ undergoes a metal-insulator transition at 630 K. This phase transition is caused by a Peierls instability normally associated with one-dimensional (1D) metals, because $Na_{0.25}TiO_2$ shows incommensurate superlattice spots centered at (a^*, q_{b^*}, 0) below 430 K.[1,2] The q_{b^*} value of this charge density wave (CDW) is found to increase gradually from $0.230b^*$ at 430 K to $0.245b^*$ at room temperature. Such a temperature dependence of CDW superlattice spot positions has been observed in molybdenum blue bronze $A_{0.3}MoO_3$ (A = K, Rb, Tl),[3,4] which contains Mo-O layers made up of MoO_6 octahedra. Since these Mo-O layers are separated by the A atoms, blue bronze has a two-dimensional structural character. However, blue bronze is a 1D metal[5] because of the way the MoO_6 octahedra are distorted in each Mo-O layer.[6] Sodium titanium bronze $Na_{0.25}TiO_2$ has a three-dimensional (3D) Ti-O lattice made up of TiO_6 octahedra,[1a] so that a particular pattern of distortion must exist in the TiO_6 octahedra for the 3D Ti-O lattice to have a 1D metallic character. Thus it is important to understand how the electronic structure of $Na_{0.25}TiO_2$ is related to its crystal structure. The main objective of the present study is to examine this structure-property relationship. In the following, we first describe the crystal structure of $Na_{0.25}TiO_2$ from the viewpoint of TiO_6 octahedra and then analyze its tight-binding band electronic structure[7] calculated by the extended Hückel method.[8] The atomic parameters used in our study are summarized in Table I.

Table I. Exponents ζ_i and Valence Shell Ionization Potentials H_{ii} for Slater-Type Orbitals χ_i[a,b]

χ_i	ζ_i	ζ_i'	H_{ii}, eV
Ti 3d	4.55 (0.4206)	1.40 (0.7839)	-10.81
O 2s	2.275		-32.3
O 2p	2.275		-14.8

[a] The d orbitals of Ti are given as a linear combination of two Slater type orbitals, and each is followed by a weighting factor in parentheses. [b] A modified Wolfsberg-Helmholz formula was used to calculate H_{ij}.[10]

[†] North Carolina State University.
[‡] Université de Nantes.

(1) (a) Brohan, L. Ph.D. Thesis, Université Nantes, 1986. (b) Brohan, L.; Marchand, R.; Tournoux, M. *J. Solid State Chem.* **1988**, *72*, 145.
(2) Colaitis, D.; Coene, W.; Amelinckx, S.; Brohan, L.; Marchand, R. *J. Solid State Chem.* **1988**, *75*, 156.
(3) (a) Pouget, J. P.; Noguera, C.; Moudden, A. H.; Moret, T. *J. Phys.* (*Les Ulis, Fr.*) **1985**, *46*, 1731. (b) Pouget, J. P.; Kagoshima, S.; Schlenker, C.; Marcus, J. *J. Phys. Lett.* **1983**, *44*, 6133. (c) Fleming, R.; Schneemeyer, L. F.; Moncton, D. E. *Phys. Rev. B* **1988**, *31*, 899. (d) Tamegai, T.; Tsutsumi, K.; Kagoshima, S.; Kanai, Y.; Taui, M.; Tomozawa, H.; Sato, M.; Tsuji, K.; Harada, J.; Sakata, M.; Nakajima, T. *Solid State Commun.* **1984**, *51*, 585.
(4) (a) Ghedira, M.; Chenavas, J.; Marezio, M.; Marcus, J. *J. Solid State Chem.* **1985**, *57*, 300. (b) Ganne, M.; Boumaza, A.; Dion, M.; Dumas, J. *Mater. Res. Bull.* **1988**, *20*, 1297. (c) Graham, J.; Wadsley, A. D. *Acta Crystallogr.* **1966**, *20*, 93.
(5) Whangbo, M.-H.; Schneemeyer, L. F. *Inorg. Chem.* **1986**, *25*, 2424.

0020-1669/90/1329-1413$02.50/0